journal

J. Am. Ceram. Soc., 84 [7] 1453–58 (2001)

Synthesis of Ultrafine Ceria Powders by Mechanochemical Processing

Takuya Tsuzuki† and Paul G. McCormick†

Research Center for Advanced Mineral and Materials Processing, The University of Western Australia, Nedlands, Perth, Western Australia 6907, Australia

The synthesis of ultrafine cerium dioxide (CeO_2) powders via mechanochemical reaction and subsequent calcination was studied. Anhydrous $CeCl_3$ and NaOH powders, along with NaCl diluent, were mechanically milled. A solid-state displacement reaction—$CeCl_3 + 3NaOH \rightarrow Ce(OH)_3 + 3NaCl$—was induced during milling in a steady-state manner. Calcination of the as-milled powder in air at 500°C resulted in the formation of CeO_2 nanoparticles in the NaCl matrix. A simple washing process to remove the NaCl yielded CeO_2 particles ~10 nm in size. The particle size was controlled in the range of ~10–500 nm by changing the calcination temperature.

I. Introduction

RECENTLY, cerium oxide (CeO_2) has attracted much attention, because of its many practical uses, such as chemical mechanical polishing media,[1] automobile exhaust catalysts,[2] additives in ceramics such as zirconium-toughened alumina to enhance sintering properties,[3] and solid electrolytes in solid oxide fuel cells.[4] Ultrafine powder is particularly important for many of these applications, because of its small size, high surface area, and improved sintering properties.

The usual method for the production of fine CeO_2 powders is a thermal decomposition of cerium salt precursors such as hydroxide, carbonate, and oxide hydrate that have been derived from sol–gel routes or wet chemical precipitation.[5,6] Although very porous powders with high surface areas are produced using this method, the minimum particle size obtained is limited to micrometer sizes, because of aggregation during thermal decomposition.[7–9] Several decomposition methods to avoid the agglomeration have been studied. Levin *et al.*[10] used a vibrational–thermal method, i.e., dynamic thermal decomposition of cerium carbonate. Mani *et al.*[11] used a sol-spray technique. However, the mean particle sizes were still >100 nm.

Various other methods of synthesizing ultrafine CeO_2 powder have been investigated.[12] Flash-combustion synthesis that involves the rapid decomposition of a saturated aqueous solution containing ceric ammonium nitrate and urea is suitable for large-quantity production. However, this method yields large particle sizes (~1 μm), which makes the application of nanoparticle synthesis difficult.[13,14] Hydrothermal synthesis, which involves precipitation from aqueous solutions under elevated temperature and pressure, has been used to produce CeO_2 nanoparticles 10–20 nm in size. However, this method requires heat treatment for several hours under high pressure (10–100 MPa).[15–19] A wet chemical precipitation method has been successfully used to synthesize semiconductor quantum dots[20,21] and has been applied to the production of CeO_2 nanoparticles. For example, Chen *et al.*[22] used a homogeneous precipitation method to directly precipitate CeO_2 particles ~70 nm in size. Masui and co-workers[23,24] used a microemulsion method to obtain separated CeO_2 nanoparticles ~4 nm in size. However, application of the method to industrial production is limited, because of the low yield rate. An inductively coupled plasma spray (spray-ICP) technique has been applied to synthesize materials with high melting points; Suzuki *et al.*[25] produced geometrically shaped CeO_2 that was <50 nm in size, but only at a low yield rate. A method to synthesize nanophase CeO_2 with high surface area and small particle size is still under intense investigation.

Recently, mechanochemical processing has been applied for the synthesis of a wide range of nanoparticulate materials.[26,27] Ding and co-workers[28–34] reported the synthesis of nanoparticles of several transition metals and ceramics, such as Al_2O_3, ZrO_2, Fe_2O_3, and ZnS; this group of researchers used a novel method that involved mechanical activation of the solid-state displacement reactions to synthesize these nanoparticles. Milling of the precursor powders leads to the formation of a nanoscale composite structure of the starting materials that react during milling or subsequent heat treatment to form a mixture of separated nanocrystals of the desired phase within a soluble salt matrix. For example, ultrafine ZrO_2 powder was synthesized via the milling and subsequent heat treatment of a mixture of $ZrCl_4$ and CaO powder. The displacement reaction, $ZrCl_4 + 2CaO \rightarrow ZrO_2 + 2CaCl_2$, was induced in a steady-state manner, forming ZrO_2 nanoparticles within a $CaCl_2$ matrix. Removal of the $CaCl_2$ by-product with a simple washing process resulted in separated ZrO_2 particles ~5 nm in size.[32]

An investigation of the synthesis of rare-earth-oxide nanoparticles via mechanochemical processing was conducted for Gd_2O_3 via the reaction $2GdCl_3 + 3CaO \rightarrow Gd_2O_3 + 3CaCl_2$.[35] However, only large particles (100 nm in size) were obtained, because of the complicated reaction route: GdOCl was formed during milling, and the reaction $6GdOCl + 2Ca_4OCl_6 + CaO \rightarrow 3Gd_2O_3 + 9CaCl_2$ occurred only during heat treatment at high temperature. Therefore, the above-described reaction was not suitable for the synthesis of nanosized Gd_2O_3 particles. Furthermore, reactions between a rare-earth chloride and an alkali-earth oxide cannot be applied to synthesize light-rare-earth oxides such as La_2O_3, CeO_2, Pr_2O_3, Nd_2O_3, and Sm_2O_3, because of the high stability of rare-earth oxychlorides. The change in free energy in the reaction $2ROCl + CaO \rightarrow R_2O_3 + CaCl_2$ (where R is a rare-earth element) is positive for lightweight lanthanides such as lanthanum, neodymium, and samarium; however, the change in free energy is negative for gadolinium and the heavier lanthanides.

As an alternative route for the synthesis of rare-earth-oxide nanoparticles, the mechanochemical reaction $GdCl_3 + 3NaOH \rightarrow Gd(OH)_3 + 3NaCl$ and a subsequent calcination was studied.[36] The solid-state displacement reaction $GdCl_3 + 3NaOH \rightarrow Gd(OH)_3 + 3NaCl$ was induced during milling, and calcination of the as-milled powder at 500°C led to the formation of Gd_2O_3 particles. The addition of a sufficient amount of NaCl diluent in the starting powder resulted in the formation of ultrafine Gd_2O_3 particles ~20 nm in size.

In this paper, we report a study of the synthesis of CeO_2 nanoparticles via the mechanochemical reaction $CeCl_3 + 3NaOH \rightarrow$

I-W. Chen—contributing editor

Manuscript No. 189146. Received August 23, 1999; approved March 27, 2000.

†Present address: Advanced Nano Technologies Pty., Ltd., Welshpool, Western Australia 6106, Australia.

$Ce(OH)_3$ + 3NaCl and a subsequent calcination. The effect of calcining temperature on particle size was also investigated.

II. Experimental Procedure

The starting materials were anhydrous $CeCl_3$ powder (99.9% pure, −20 mesh; Cerac, Milwaukee, WI), NaOH (99.99% pure, in pellet form; Aldrich, Milwaukee, WI), and NaCl (99.8% pure, in the form of beads; Sigma, St. Louis, MO). The $CeCl_3$ and NaCl powders were dried under vacuum at 200°C before use. The mixture of starting powders was sealed in a hardened-steel vial with hardened-steel balls 6.4 mm in diameter, under a high-purity argon-gas atmosphere. Milling was performed with a mixer/mill (Model 8000, Spex, Edison, NJ), using a ball-to-powder mass ratio of 10:1. To detect possible combustion events,[37,38] the surface temperature of the vial was measured during milling, using a thermocouple that was attached to the outside surface of the vial. Calcination and annealing of the as-milled powder were conducted in an alumina crucible in air for 0.5 h. Removal of the NaCl by-product was performed by washing the powder with deionized water, using an ultrasonic bath and a centrifuge. The washed powder was dried in an oven (at 60°C) for several hours.

The structure of the powder was examined under an argon-gas atmosphere at room temperature via X-ray diffractometry (XRD) (Model D5000, Siemens, Karlsruhe, Germany), using Cu$K\alpha$ radiation. The mean crystallite size of the powder was estimated from the diffraction-peak width, using the Scherrer equation.[39] The microstructure of the powder was studied via transmission electron microscopy (TEM) (Model 430, Philips, Eindhoven, the Netherlands and Model 2000 FXII, JEOL, Tokyo, Japan, the latter of which was equipped with a energy-dispersive spectroscopy (EDS) system (Link Systems, High Wycombe, Buckinghamshire, U.K.)). For the TEM studies, the washed powder was dispersed in methanol using an ultrasonic bath and a drop of solution was placed on a copper grid that had been coated with holey carbon film. Simultaneous differential thermal analysis (DTA) and thermogravimetric analysis (TGA) were conducted using a thermal analysis system (Model Thermoflex, Rigaku, Tokyo, Japan) under a constant air flow of 2 cm^3/min with a heating rate of 20°C/min. The specific surface area was measured via a Brunauer–Emmett-Teller (BET) nitrogen-gas absorption method at a temperature of 77 K (Model Gemini 2360, Micromeritics, Norcross, GA). The particle size was also measured via a laser light scattering (LLS) method (Model Mastersizer Microplus, Malvern Instruments, Malvern, U.K.). For the LLS measurements, powders were dispersed in deionized water with a $(NaPO_3)_6$ dispersant, using an ultrasonic probe for >15 min. A density of 7.135 g/cm^3 and real and imaginary parts of the refractive index—2.3 and 0.1, respectively—were used for the LLS measurements. Inductively coupled plasma–atomic emission spectroscopy (ICP–AES) analysis was conducted at the Chemistry Centre at the University of Western Australia, to analyze the CeO_2 nanopowder for traces of elemental iron, sodium, and chlorine.

III. Results and Discussion

(1) Mechanochemical Reaction of $CeCl_3$ and NaOH

An abrupt increase in the vial temperature was observed after a powder mixture of $CeCl_3$ and 3 mol of NaOH was milled for ~40 s. This phenomenon indicates that a self-propagating exothermal reaction (combustion) occurred during milling; this reaction was due to the large negative enthalpy change (−345 kJ)[40,41] of the reaction

$$CeCl_3 + 3NaOH \rightarrow Ce(OH)_3 + 3NaCl \quad (1)$$

The milling was terminated 2 min after the combustion event. The powder obtained was attached to the inside of the vial as a hard cake and was difficult to recover. The XRD pattern of the powder consisted of peaks that corresponded to $Ce(OH)_3$ and NaCl, as shown in pattern "(a)" in Fig. 1. Therefore, because of the combustion event, the reaction was completed within a short time.

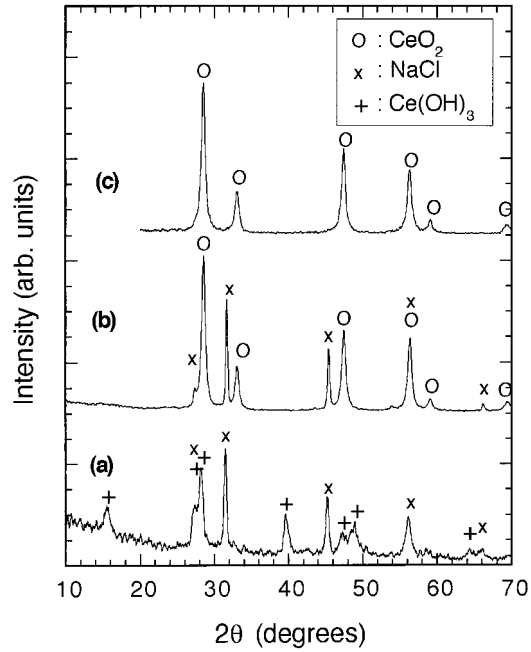

Fig. 1. XRD patterns of the $CeCl_3$ + 3NaOH powder mixture without NaCl diluent ((a) as-milled powder after combustion, (b) powder calcined at 500°C, and (c) powder washed after calcining).

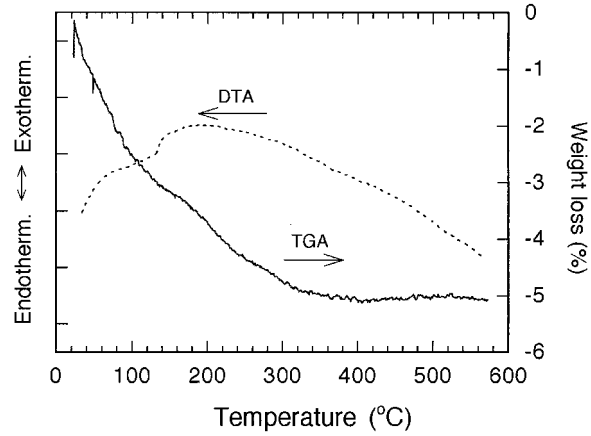

Fig. 2. TG/DTA curves of the as-milled $CeCl_3$ + 3NaOH powder mixture after combustion.

To determine the decomposition temperature of the synthesized $Ce(OH)_3$, simultaneous TGA and DTA measurements of the as-milled powder were conducted. Figure 2 shows DTA and TGA curves for the as-milled powder. The TGA curve shows that the powder mass started to decrease as the temperature increased from room temperature and attained a constant value at a temperature of ~350°C. Although a weak hump was observed at ~170°C, there was no clear evidence of a two-step decomposition, as in the case of $Gd(OH)_3$.[34] The calculated weight loss for the reaction

$$Ce(OH)_3 + 0.25O_2 \rightarrow CeO_2 + 1.5H_2O \quad (2)$$

during heat treatment is 5.2 wt%. The measured weight loss was ~5%, which is almost the same as the calculated value. The air atmosphere was the oxygen source in reaction (2). The gradient of the DTA curve showed a gradual change in the temperature range between 20°C and 350°C, possibly due to the gradual change in the specific heat of the powder during reaction (2). It is not clear whether the kink at 130°C in the DTA curve is due to an

endothermic peak at ~120°C or a broad exothermic peak from 140°C to 350°C.

The as-milled powder was heat-treated at 500°C for 0.5 h in air. Pattern "(b)" in Fig. 1 shows an XRD pattern of the powder after heat treatment. $Ce(OH)_3$ evidently was converted to CeO_2 during heat treatment via reaction (2). After the heat-treated powder was washed to remove the NaCl by-product, only the CeO_2 phase was obtained, as shown in XRD pattern "(c)" in Fig. 1.[42]

Figure 3 shows a typical TEM image of the CeO_2 powder that was obtained. The powder consisted of particles 100-1000 nm in size, which were aggregates of crystallites 10–30 nm in size. The mean crystallite size, as estimated from XRD peak broadening, was 12.5 nm, which is in good agreement with the crystallite sizes observed via TEM. The large particle size is due to the high temperature induced by the combustion event,[28,30,38] as well as being due to the low volume ratio of NaCl to $Ce(OH)_3$ in the product phase ($NaCl:Ce(OH)_3 = 2.2:1$).[34]

The BET specific surface area of the powder was 64.5 m^2/g. The particles could not be separated as spherical crystallites with a smooth surface (Fig. 3); therefore, the mean particle size was not calculated from the BET surface area. The high BET surface area was due to the porous structure of the aggregates.

(2) Effect of Diluent

To investigate the effect of diluent on the mechanochemical reaction, a NaCl diluent was added in the starting powder mixture. A stoichiometric mixture of starting powders that corresponded to the reaction equation

$$CeCl_3 + 3NaOH + 12NaCl \rightarrow Ce(OH)_3 + 15NaCl \qquad (3)$$

was milled for different times. The addition of 12 mol of NaCl to the reactants increased the volume fraction of NaCl in the product phase mixture to 90%.

No combustion was detected during the milling of a powder mixture of $CeCl_3$, 3 mol of NaOH, and 12 mol NaCl. The NaCl diluent prevented combustion from occurring, because of the following reasons: (i) NaCl separated the reactants, which reduced the collision frequency between the reactant particles and led to a decrease in the reaction rate and the rate of heat generation; (ii) NaCl absorbed the collision energy during milling, which reduced the energy that was transferred to the reactants; and (iii) NaCl absorbed the heat that was generated by the reaction, which prevented the excess increase in temperature during milling.

Figure 4 shows XRD patterns of the powder that was milled for various times. As the milling time increased, the peaks associated with $CeCl_3$ were gradually weakened, whereas the intensity of the peaks associated with $Ce(OH)_3$ increased. This observation indicates that a solid-state displacement reaction occurred during milling in a steady-state manner. After milling for 2 h, the XRD pattern consisted of peaks that were associated with $Ce(OH)_3$ and NaCl. The width of the peaks that corresponded to $Ce(OH)_3$ became narrower as the milling time increased from 2 h to 4 h. The mean crystallite size of $Ce(OH)_3$ in the powder milled for 4 h, which was estimated from the XRD pattern using a peak at ~40°, was 10 nm.

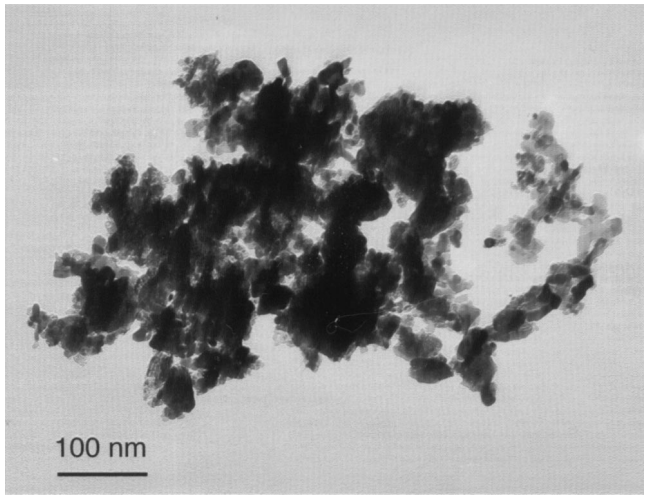

Fig. 3. TEM image of the CeO_2 powder after calcination at 500°C and subsequent washing.

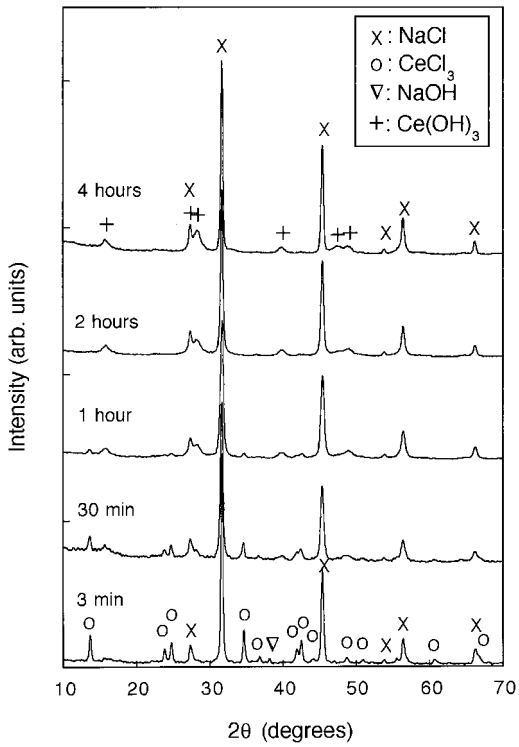

Fig. 4. XRD patterns of the $CeCl_3 + 3NaOH + 12NaCl$ powder mixture milled for different times. Milling times are indicated in the figure.

Following the results of TG/DTA measurements in section III*(1)*, the as-milled powder was calcined at 500°C and subsequently washed to remove NaCl. XRD measurements confirmed that only the CeO_2 phase was obtained after washing. The mean crystallite size, as estimated from the XRD peak widths, was 10.2 nm.

TEM analysis of the calcined and subsequently washed powder has shown that the particles sizes were 5–40 nm and that only weak agglomeration of the particles was observed (see related image in Fig. 6(a)). Dark-field imaging revealed that each particle was a single crystal. No traces of sodium, chlorine, or iron were detected using EDS. ICP–AES analysis detected the presence of iron (0.023 wt%), sodium (0.244 wt%), and chlorine (0.045 wt%) in the CeO_2 nanopowder.

The BET surface area of the calcined and washed powder was 83 m^2/g, which corresponds to a spherical particle size of 10 nm. This finding is in good agreement with the results of XRD and TEM analyses. Because of the addition of the NaCl diluent, the $Ce(OH)_3$ particles were well isolated from each other in the NaCl matrix, which led to the formation of CeO_2 particles as small as ~10 nm.[34,36]

(3) Particle Growth

The as-milled $CeCl_3 + 3NaOH + 12NaCl$ powder mixture was calcined at temperatures of 500°–1000°C and subsequently washed to remove NaCl. Figure 5 shows the XRD crystallite size, BET particle size, and LLS particle size of the CeO_2 powders, each plotted as a function of the calcining temperature. The XRD peaks of CeO_2 that was calcined at 1000°C had almost the same widths as the instrumental peak broadening; thus, accurate estimation of the crystallite size was not possible. LLS measurements for the

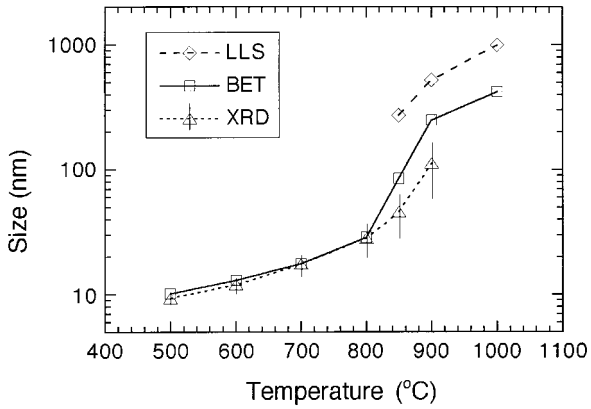

Fig. 5. (△) XRD crystallite size, (□) BET particle size, and (◇) LLS particle size of the CeO_2 particles, each as a function of the calcining temperature.

CeO_2 particles calcined at <800°C were not conducted, because the instrument could measure only particle sizes of >50 nm.

Different temperature dependences of size growth were evident below and above 800°C. Below 800°C, the XRD crystallite size and BET particle size increased rather monotonously as the temperature increased. The XRD crystallite size was almost the same as the BET particle size. This result suggests that the particles could be separated from each other, because the NaCl solid matrix isolated the CeO_2 particles from each other. Above 800°C, the XRD crystallite size and BET particle size increased more rapidly than they did at <800°C. The BET particle size increased more rapidly than the XRD crystallite size, and, after calcining at 900°C, was more than twice the XRD crystallite size. The difference between these sizes will be discussed later. The higher rate of particle-size growth at temperatures above 800°C than that at temperatures below 800°C is due to the molten NaCl matrix: the melting point of NaCl is 801°C, and sedimentation of CeO_2 particles was observed after heat treatment above this temperature. This sedimentation caused the particles to come into contact with each other, which led to rapid particle growth.

Figures 6(a)–(d) show TEM images of powder that has been calcined at different temperatures. CeO_2 particles that have been synthesized via calcination at 500°C consisted of equiaxed particles 5–40 nm in size (Fig. 6(a)). CeO_2 particles that have been synthesized via calcination at 800°C were spherical and 10–130 nm in size (Fig. 6(b)). This result is in good agreement with the XRD crystallite size and BET particle size observed at these temperatures. Loose agglomerations were evident in the TEM images, which was consistent with the fact that the XRD crystallite size was almost the same as the BET particle size, which suggests that the particles could be separated from each other. The TEM micrograph in Fig. 6(b) showed a rather-wide particle-size distribution, which was possibly due to Ostwald ripening. However, the

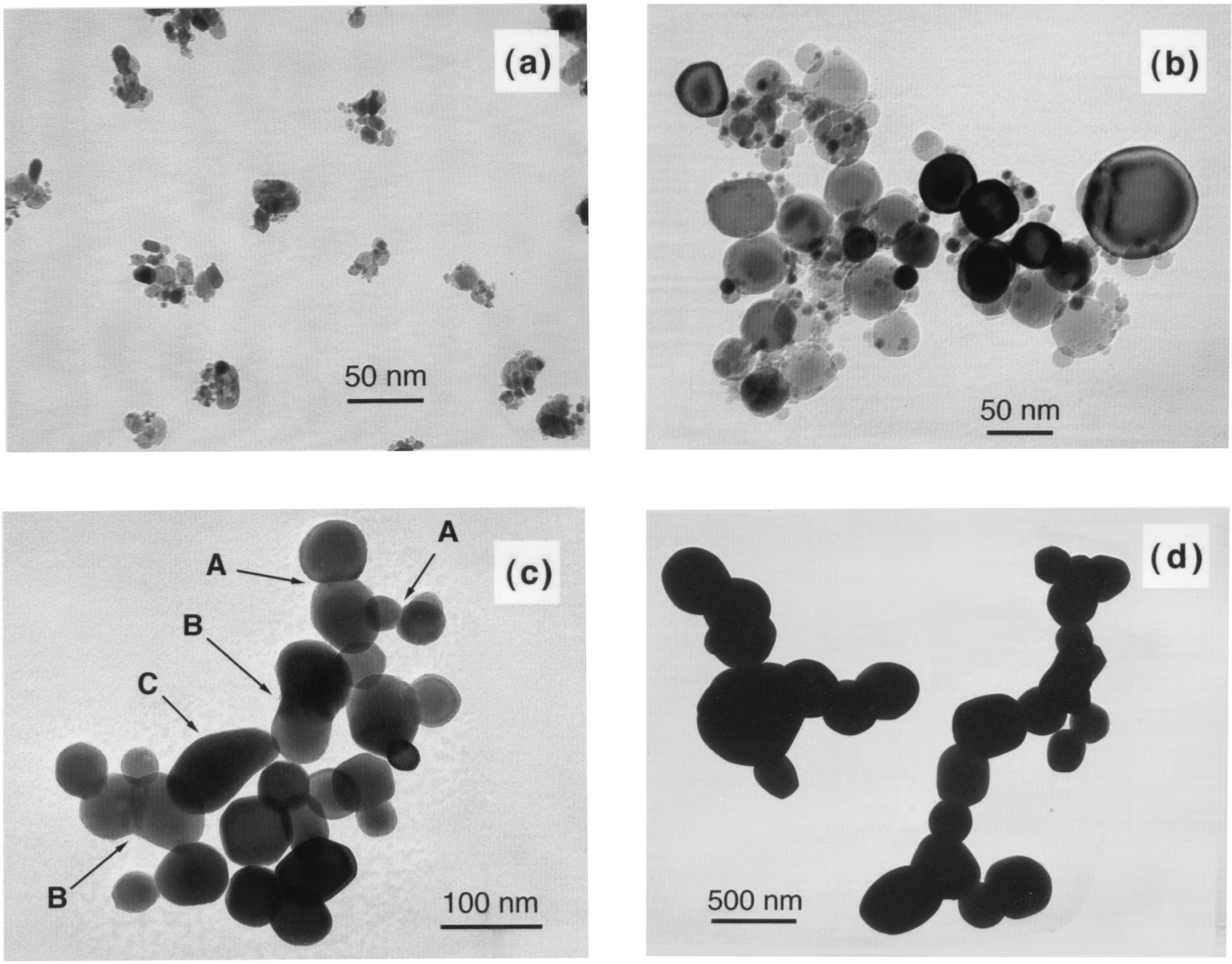

Fig. 6. TEM image of the CeO_2 nanoparticles obtained from $CeCl_3$ + 3NaOH + 12NaCl mixture powders, calcined at (a) 500°, (b) 800°, (c) 850°, and (d) 1000°C.

extensive overlapping of the particles in the images made estimation of the actual size distribution from the TEM images difficult.

Figure 6(c) shows CeO_2 particles that have been obtained via calcination at 850°C. Different stages of particle growth are evident. First, the particles are in contact with each other, sharing facets as indicated by feature "A" in Fig. 6(c). Second, some particles seem to form necks between them and have sintered together (feature "B" in Fig. 6(c)). The different contrast in the two sintering particles suggests that the particles still retain different crystal orientations. Finally, the neck disappears and a single crystallite is formed (feature "C" in Fig. 6(c)). Therefore, above 800°C, some particles could not be separated from each other anymore, because of the first and second stage of the particle growth due to interparticle sintering, which reduces the BET surface area and leads to the BET particle size becoming larger than the XRD crystallite size.

The LLS size distributions for the powders that have been calcined at 850°, 900°, and 1000°C are shown in Fig. 7. The LLS particle size of the powder calcined at 850°C was ~230 nm, which is much larger than the XRD crystallite size (45.7 nm) and the BET particle size (84.7 nm). The same tendency in the difference between XRD, BET, and LLS particle sizes was observed for the powders that were calcined at 900° and 1000°C. This observation is due to the nonspherically shaped aggregates of sintered particles such as those labeled A, B, and C in Fig. 6(c). The general tendency when using LLS size distributions of nonspherical particles is to oversize the coarse end of the distribution, because LLS uses the longer axis of an elongated particle to determine the mean particle diameter.[43] Another reason for obtaining a larger LLS size is that the fundamental size distribution, as derived via LLS, is based on volume; in other words, if a sample consists of an equal number of two sizes of particles, e.g., 50 nm and 100 nm, the volume of the 100-nm particles is 8 times larger than that of the 50-nm particles. Hence, as a volume distribution, the larger particles represent most of the total volume, which yields a mean particle size (as a peak position of the size distribution) by volume that is larger than that obtained by population.

The sintering process of nanosized single crystals is very important in powder processing. The kinetics of grain growth consist of two regimes, i.e., sintering and subsequent coarsening.[44–48] The first regime (sintering) is described as follows. For small particles, surface diffusion is the dominant mass-transport mechanism. Negative surface curvature provides a more-stable environment to the mass on the surface than positive surface curvature; thus, the gap between the contacting particles is filled by the mass. Hence, if the particles are crystals, a grain boundary forms at the expense of surface energy. The neck radius attains a maximum static size, because of the equilibrium between grain-boundary energy and surface energy. In the second regime (coarsening), when adjacent sintered particles have different sizes, mass transport is induced from the smaller particle to the larger one, because of the difference in the surface curvature. This phenomenon leads to the absorption of the smaller particle by the larger one, with a grain boundary retained between them.

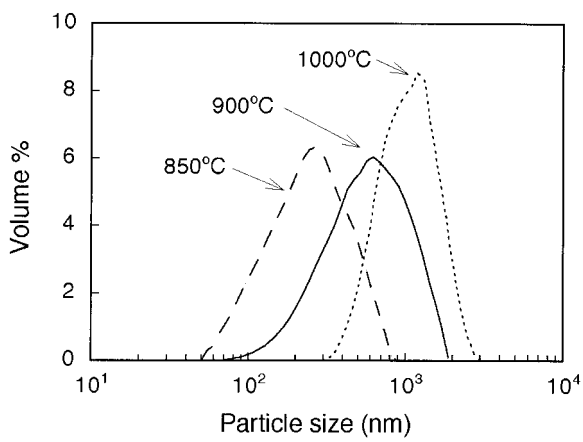

Fig. 7. LLS size distribution of the CeO_2 nanoparticles obtained from $CeCl_3$ + 3NaOH + 12NaCl powder mixtures, calcined at (– – –) 850°, (—) 900°, and (· · ·) 1000°C.

This general model of two-particle sintering is phenomenological and mostly based on *ex situ* observation of large (micrometer-sized) particle sintering.[44–50] However, the sintering properties of nanoparticles may be different from those of micrometer-sized particles. Moreover, *ex situ* TEM study has shown only sintering properties that have been averaged over the heating time. Recently, many *in situ* TEM studies of nanoparticle sintering have been conducted.[51–53] Averback and co-workers[54–56] performed a molecular-dynamics simulation of the free sintering of nanosized TiO_2 particles, as well as an *in situ* TEM study of the sintering of copper and silver nanoparticles. Sintered nanoparticle pairs reoriented themselves, with respect to each other, in the coarsening regime, forming a low-energy grain boundary. This particle reorientation during coarsening was also observed by Rankin *et al.*[57] in ZrO_2 nanoparticles ~30 nm in size that were loosely attached to a carbon film on a TEM grid. However, when the ZrO_2 nanoparticles were fixed to the TEM grid, the coarsening occurred via the absorption of smaller particles by larger ones, while a grain boundary was maintained between them.[52]

In the present study, CeO_2 nanoparticles formed nonspherical, sintered single crystallites, as shown by feature C in Fig. 6(c). This finding suggests that the grain boundary between two sintered particles disappeared before the smaller particle was absorbed by the larger one; i.e., coarsening occurred via particle reorientation. The particles were suspended in molten NaCl; thus, particle rotation, to minimize the grain-boundary energy, was possible.

IV. Summary

A solid-state displacement reaction between $CeCl_3$ and NaOH was induced by mechanochemical processing, forming $Ce(OH)_3$ in a NaCl matrix. Ultrafine CeO_2 powders were obtained after the as-milled powders were calcined. A simple washing process was used to remove the NaCl by-product/diluent. Without any addition of NaCl diluent, calcination of the mechanochemically synthesized $Ce(OH)_3$ resulted in the formation of porous CeO_2 particles 0.1–1 μm in size. Although the particle size is rather large, the porous structure gave a high BET surface area. Milling with NaCl diluent led to the formation of CeO_2 nanoparticles ~10 nm in size, because the mechanochemically formed hydroxide precursors were well isolated in the NaCl matrix, which prevented the particles from sintering together during thermal decomposition. Therefore, to obtain particles ~10 nm in size, it is necessary to cause a reaction in a steady-state manner, as well as to increase the matrix:powder volume ratio. The mean particle size was controlled in the range of 10–500 nm by varying the calcination temperature. Almost-spherical particles were obtained after calcination at temperatures of >800°C. The difference between particle sizes obtained using XRD, BET, and LLS methods has been demonstrated to be a good indicator of particle aggregation. This synthesis method has potential for the economical and efficient production of ultrafine rare-earth-oxide powders.

References

[1]N. B. Kirk and J. V. Wood, "Glass Polishing," *Br. Ceram. Trans.*, **93** [1] 25–30 (1994).

[2]B. R. Powell, R. L. Bloink, and C. C. Erckel, "Preparation of Cerium Dioxide Powders for Catalyst Supports," *J. Am. Ceram. Soc.*, **71** [2] C-104–C-106 (1988).

[3]S. B. Bhaduri, A. Chakraborty, and R. M. Rao, "Method of Fabricating Ceria-Stabilized Tetragonal Zirconia Polycrystals," *J. Am. Ceram. Soc.*, **71** [9] C-410–C-411 (1988).

[4]J. Van herle, T. Horita, T. Kawata, N. Sakai, H. Yokokawa, and M. Dokiya, "Fabrication and Sintering of Fine Yttria-Doped Ceria Powder," *J. Am. Ceram. Soc.*, **80** [4] 933–40 (1997).

[5]G. A. M. Hussein, "Rare Earth Metal Oxides: Formation, Ccharacterization and Catalytic Activity, Thermoanalytical and Applied Pyrolysis Review," *J. Anal. Appl. Pyrolysis*, **37**, 111–49 (1996).

[6]B. Djuricic and S. Pickering, "Nanostructured Cerium Oxide: Preparation and Properties of Weakly-Agglomerated Powders," *J. Eur. Ceram. Soc.*, **19**, 1925–34 (1999).

[7]X. Chu, W. Chung, and L. D. Shmidt, "Sintering of Sol–Gel Prepared Submicrometer Particles Studied by Transmission Electron Microscopy," *J. Am. Ceram. Soc.*, **76** [8] 2115–18 (1993).

[8]E. Matijevic and W. P. Hsu, "Preparation and Properties of Monodispersed Colloidal Particles of Lanthanide Compounds: I. Gadolinium, Europium, Terbium, Samarium and Cerium(III)," *J. Colloid Interface Sci.*, **118** [2] 506–23 (1987).

[9]J. M. Heintz and J. C. Bernier, "Synthesis and Sintering Properties of Cerium Oxide Powders Prepared from Oxalate Precursors," *J. Mater. Sci.*, **21** [5] 1569–73 (1986).

[10]M. I. Levin, E. A. Bondarenko, N. L. Nazarova, S. S. Kulagina, and E. E. Belousova, "Vibrational–Thermal Method of Obtaining Finely Dispersed Cerium Dioxide," *Sov. J. Opt. Technol.*, **58** [2] 118–20 (1991).

[11]T. V. Mani, H. K. Varma, A. D. Damodaran, and K. G. K. Warrier, "Sol-Spray Technique for Fine-Grained Ceria Particles," *Ceram. Int.*, **19** [2] 125–28 (1993).

[12]G. Adachi and N. Imanaka, "The Binary Rare Earth Oxides," *Chem. Rev.*, **98**, 1479–514 (1998).

[13]M. M. A. Sekar, S. S. Manoharan, and K. C. Patil, "Combustion Synthesis of Fine-Particle Ceria," *J. Mater. Sci. Lett.*, **9** [10] 1205–206 (1990).

[14]H. K. Varma, P. Mukundan, K. G. K. Warrier, and A. D. Damodaran, "Flash Combustion Synthesis of Cerium Oxide," *J. Mater. Sci. Lett.*, **9** [4] 377–79 (1990).

[15]K. Hakuta, S. Onai, H. Terayama, T. Adshiri, and K. Arai, "Production of Ultra-fine Ceria Particles by Hydrothermal Synthesis under Supercritical Conditions," *J. Mater. Sci. Lett.*, **17**, 1211–13 (1998).

[16]M. Hirano and E. Kato, "The Hydrothermal Synthesis of Ultrafine Cerium(IV) Oxide Powders," *J. Mater. Sci. Lett.*, **15**, 1249–50 (1996).

[17]M. Hirano and E. Kato, "Hydrothermal Synthesis of Cerium(IV) Oxide," *J. Am. Ceram. Soc.*, **79** [3] 777–80 (1996).

[18]C. Wang, Y. Qian, X. Yi, C. Wang, Y. Li, and G. Zhao, "A Novel Method to Prepare Nanocrystalline (7 nm) Ceria," *Mater. Sci. Eng. B*, **B39** [3] 160–62 (1996).

[19]Y. C. Zhou and M. N. Rahaman, "Hydrothermal Synthesis and Sintering of Ultrafine CeO_2 Powders," *J. Mater. Res.*, **8** [7] 1680–86 (1993).

[20]C. B. Murray, D. J. Norris, and M. G. Bawendi, "Synthesis and Characterization of Nearly Monodispersed CdE (E = S, Se, Te) Semiconductor Nanocrystallites," *J. Am. Chem. Soc.*, **115**, 8706–15 (1993).

[21]A. Henglein, A. Fojtik, and H. Weller, "Reactions On Colloidal Semiconductor Particles," *Ber. Bunsen—Ges. Phys. Chem.*, **91**, 441–46 (1987).

[22]P.-L. Chen and I-W. Chen, "Reactive Cerium(IV) Oxide Powders by the Homogeneous Precipitation Method," *J. Am. Ceram. Soc.*, **76** [6] 1577–83 (1993).

[23]T. Masui, K. Fujiwara, Y. Peng, T. Sakata, K. Machida, H. Mori, and G. Adachi, "Characterization and Catalytic Properties of CeO_2–ZrO_2 Ultrafine Particles Prepared by the Microemulsion Method," *J. Alloys Compd.*, **269**, 116–22 (1998).

[24]T. Masui, K. Fujiwara, K. Machida, G. Adachi, T. Sakata, and H. Mori, "Characterization of Cerium(IV) Oxide Ultrafine Particles Prepared Using Reversed Micelles," *Chem. Mater.*, **9** [10] 2197–204 (1997).

[25]M. Suzuki, M. Kagawa, Y. Syono, and T. Hirai, "Synthesis of Ultrafine Single-Component Oxide Particles by the Spray-ICP Technique," *J. Mater. Sci.*, **27**, 679–84 (1992).

[26]P. G. McCormick, J. Ding, H. Yang, and T. Tsuzuki, "Mechanochemical Synthesis of Nanostructured and Ultrafine Powder"; pp. 85–88 in *Materials Research 96*, Vol. 1. Institute of Metals and Materials Australia, Melbourne, Australia, 1996.

[27]G. B. Schaffer and P. G. McCormick, "Mechanical Alloying," *Mater. Forum*, **16**, 91–97 (1992).

[28]J. Ding, W. F. Miao, P. G. McCormick, and R. Street, "Mechanochemical Synthesis of Ultrafine Fe Powder," *Appl. Phys. Lett.*, **67** [25] 3804–806 (1995).

[29]J. Ding, T. Tsuzuki, P. G. McCormick, and R. Street, "Ultrafine Cu Particles Prepared by Mechanochemical Process," *J. Alloys Compd.*, **234**, L1–L3 (1996).

[30]J. Ding, T. Tsuzuki, P. G. McCormick, and R. Street, "Ultrafine Co and Ni Particles Prepared by Mechanochemical Processing," *J. Phys. D: Appl. Phys.*, **29** [9] 1365–69 (1996).

[31]J. Ding, T. Tsuzuki, and P. G. McCormick, "Ultrafine Alumina Particles Prepared by Mechanochemical/Thermal Processing," *J. Am. Ceram. Soc.*, **79** [11] 2956–58 (1996).

[32]J. Ding, T. Tsuzuki, and P. G. McCormick, "Mechanochemical Synthesis of Ultrafine ZrO_2 Powder," *Nanostruct. Mater.*, **8** [1] 75–81 (1997).

[33]J. Ding, T. Tsuzuki, and P. G. McCormick, "Hematite Powders Synthesized by Mechanochemical Processing," *Nanostruct. Mater.*, **8** [6] 739–47 (1997).

[34]T. Tsuzuki, J. Ding, and P. G. McCormick, "Mechanochemical Synthesis of Ultrafine Zinc Sulfide Particles," *Physica B (Amsterdam)*, **239**, 378–87 (1997).

[35]T. Tsuzuki, W. T. A. Harrison, and P. G. McCormick, "Synthesis of Ultrafine Gadolinium Oxide Powder by Mechanochemical Processing," *J. Alloys Compd.*, **281**, 146–51 (1998).

[36]T. Tsuzuki, E. Pirault, and P. G. McCormick, "Mechanochemical Synthesis of Gadolinium Oxide Nanoparticles," *Nanostruct. Mater.*, **11** [1] 125–31 (1999).

[37]G. B. Schaffer and P. G. McCormick, "On the Kinetics of Mechanical Alloying," *Metall. Trans. A*, **A23**, 1285–90 (1992).

[38]H. Yang and P. G. McCormick, "Combustion Reaction of Zinc Oxide with Magnesium during Mechanical Milling," *J. Solid State Chem.*, **107**, 258–63 (1993).

[39]B. D. Cullity, *Elements of X-ray Diffraction*, 2nd Ed.; p. 102. Addison–Wesley, Reading, MA, 1978.

[40]T. L. Woods and R. M. Garreels, *Thermodynamic Values at Low Temperature for Natural Inorganic Materials*; p. 68. Oxford University Press, New York, 1987.

[41]I. Barin Ed., *Thermodynamic Data of Pure Substances*, 2nd Ed.; pp. 376, 982, and 990. VCH, Weinheim, Germany, 1993.

[42]Powder Diffraction File Card No. 34-395, Joint Committee for Powder Diffraction Standards (JCPDS), Swarthmore, PA (now International Centre for Diffraction Data (ICDD), Newtown Square, PA).

[43]T. Allen, *Particle Size Measurement*, Vol. 1, 5th Ed.; pp. 404–19. Chapman and Hall, New York, 1997.

[44]F. F. Lange and B. J. Kellett, "Thermodynamics of Densification, II. Grain Growth in Porous Compacts and Relation to Densification," *J. Am. Ceram. Soc.*, **72** [5] 735–41 (1989).

[45]B. J. Kellett and F. F. Lange, "Thermodynamics of Densification, I. Sintering of Simple Particle Arrays, Equilibrium Configurations, Pore Stability, and Shrinkage," *J. Am. Ceram. Soc.*, **72** [5] 725–34 (1989).

[46]W. J. Soppe, G. J. Janssen, B. C. Bonekamp, A. A. Correia, and H. J. Veringa, "A Computer Simulation Method for Sintering in Three-Dimensional Powder Compacts," *J. Mater. Sci.*, **29** [3] 754–61 (1994).

[47]F. F. Lange, "Powder Processing Science and Technology for Increased Reliability," *J. Am. Ceram. Soc.*, **72** [1] 3–15 (1989).

[48]W. Zhang and J. H. Schneibel, "The Sintering of Two Particles by Surface and Grain Boundary Diffusion—A Two Dimensional Numerical Study," *Acta Metall. Mater.*, **43** [12] 4377–86 (1995).

[49]E. B. Slamovich and F. Lange, "Densification Behavior of Single-Crystal and Polycrystalline Spherical Particles of Zirconia," *J. Am. Ceram. Soc.*, **73** [11] 3368–75 (1990).

[50]S. Ijima, "Electron Microscopy of Small Particles," *J. Electron Microsc.*, **34** [4] 249–65 (1985).

[51]J. Rankin and L. A. Boatner, "Unstable Neck Formation during Initial-Stage Sintering," *J. Am. Ceram. Soc.*, **77** [8] 1987–90 (1994).

[52]M. Kusunoki, K. Yonemitsu, Y. Sasaki, and Y. Kubo, "*In Situ* Observation of Zirconia Particles at 1200°C by High-Resolution Electron Microscopy," *J. Am. Ceram. Soc.*, **76** [3] 763–65 (1993).

[53]G. Petzow and H. E. Exner, "Particle Rearrangement in Solid State Sintering," *Z. Metallkd.*, **67** [9] 611–18 (1976).

[54]M. Yeadon, J. C. Yang, R. S. Averback, J. W. Bullard, and J. M. Gibson, "Direct Observations of the Sintering of Silver Nanoparticles on Single Crystal Copper by *In-Situ* UHV TEM"; pp. 283–88 in Materials Research Society Symposium Proceedings, Vol. 501, *Surface-Controlled Nanoscale Materials for High-Added-Value Applications*. Edited by K. E. Gonsalves, M.-I. Baraton, R. Singh, H. Hoffmann, J. X. Chen, and J. A. Akkara. Materials Research Society, Warrendale, PA, 1998.

[55]H. Zhu and R. S. Averback, "Sintering of Nano-particle Powders: Simulations and Experiments," *Mater. Manuf. Processes*, **11** [6] 905–23 (1996).

[56]R. S. Averback, H. Zhu, R. Tao, and H. Höfler, "Sintering of Nanocrystalline Materials: Experiments and Computer Simulations"; pp. 203–16 in Proceedings of the 1996 Annual Meeting of the Minerals, Metals and Materials Society, *Synthesis and Processing of Nanocrystalline Powder* (Anaheim, CA, Feb. 1996). Edited by D. L. Bourell. The Minerals, Metals and Materials Society, Warrendale, PA, 1996.

[57]J. Rankin and B. W. Sheldon, "*In Situ* TEM Sintering of Nano-Sized ZrO_2 Particles," *Mater. Sci. Eng. A*, **A204** [1–2] 48–53 (1995). □